ARTICLE

OBC
www.rsc.org/obc

Nonameric porphyrin assemblies – formation and intra-assembly energy transfer reactions

Ken Sasaki,[a] Kenji Sugou,[a] Koji Miyamoto,[a] Jyun-ichi Hirai,[a] Shigetaka Tsubouchi,[a] Hiroshi Miyasaka,[b] Akira Itaya[a] and Yasuhisa Kuroda*[a]

[a] *Department of Polymer Science, Kyoto Institute of Technology, Matsugasaki, Sakyo-ku, Kyoto 606-8585, Japan. E-mail: ykuroda@kit.ac.jp; Fax: +81-75-724-7830; Tel: +81-75-724-7830*

[b] *Department of Chemistry, Graduate School of Engineering Science, Osaka University, 1-3 Machikaneyama, Toyonaka, Osaka 560-8531, Japan*

Received 28th May 2004, Accepted 9th August 2004
First published as an Advance Article on the web 6th September 2004

The nonameric porphyrin assemblies constructed with the series of free base tetraphenylporphyrins $\mathbf{P}^n$ having four pyrazine moieties linked with alkyl chains of different lengths, $(\mathbf{CH}_2)_n$ (n = 1, 5, 9, 17, 30), and dimeric [*meso*-tetrakis(2-carboxy-4-nonylphenyl)porphyrinato]zinc(II), $\mathbf{ZnP}_2$, show the effective light-collection effect and the typical Förster-type energy transfer from $\mathbf{ZnP}_2$ to $\mathbf{P}^n$.

Introduction

The photosynthetic light-harvesting assembly is one of the most impressive molecular architectures in biological systems.[1] The highly efficient chemical reactions taking place in this assembly have been recognised as one of the ideal chemical processes and, therefore, diverse efforts to mimic this molecular system have been made for a long period.[2] Its gigantic but still well-defined structure and highly refined chemical functions provide an excellent example of the challenging subject not only for biomimetic chemistry but also for synthetic chemistry, which will lead to the exploration of new methodologies to construct artificial large-scale molecular architectures or devices. It is interesting to note that biological large-scale molecular architectures are sometimes constructed by repeated combination of a large number of smaller molecular elements by means of molecular recognition based on reversible intermolecular interactions. One typical example of such large-scale biological assemblies is the antenna complex in the photosynthetic light-harvesting system which inevitably requires many bacteriochlorophyll molecules for its functions of efficient light collection over a wide area range. For example, the recent model of the antenna system, LH2, from *Rhodopseudomonas acidophila* suggests that 27 antenna bacteriochlorophyll molecules are regularly arranged around the photoreaction centre. In spite of its gigantic structures, the total antenna system is constructed as a nonamer of a single elementary unit element containing two protein subunits and three bacteriochlorophyll moieties. These structural characteristics make the antenna systems ideal as the target for the artificial self-assembling molecular architectures.[3]

Recently we reported the construction of nonameric and heptadecameric porphyrin assemblies which show efficient light-harvesting effects and energy transfer from antenna pigments to the single central porphyrin in these assemblies.[4] These systems are constructed by using specific coordination of the pyrazine moiety on the zinc porphyrin dimer which contains tight hydrogen bonds between the carboxylic acid groups formed in the non-polar solvent such as dichloromethane.[5] It seems to be clear that the systems have not only the original advantage of the self-assembling architecture in which the large-scale molecular system is automatically generated by simple mixing of necessary components, but also another great advantage that systematic modification of their structural elements may be easily attained by rather small modification of the synthetic methods for the compounds. The latter advantage is very important for systematic investigations that clarify the mechanistic details of the chemical processes occurring in multi-component, large-scale assemblies. In this article, we describe the spectroscopic and kinetic characteristics of the series of nonameric porphyrin assemblies that have different lengths of alkyl chains linking the antenna porphyrins with the central acceptor porphyrin.

Results

Preparation of central free base porphyrins bearing four pyrazine moieties

Our previous investigations reveal that the main photochemical characteristics of the present type of porphyrin assemblies are susceptible to the distance between the component porphyrins but not so sensitive to the nature of chemical bonds connecting the components.[4] For the purpose of systematic investigation of the antenna effect, we designed a series of TPP derivatives bearing the antenna positions connected with ether linkages of different alkyl chain lengths. The synthetic scheme of the present central free base porphyrins is shown in Scheme 1. These simple synthetic procedures are clearly advantageous for the preparation of a series of porphyrin derivatives that should be constructed with the common core porphyrin and easily available alkylpyrazine components. Three bromoalkylpyrazines having penta-, nona- and hepta-decamethylene moieties were prepared by the reaction of the pyrazinyllmethyl anion with the corresponding dibromoalkane.[6] The shortest bromoalkylpyrazine, 2-bromomethylpyrazine, was obtained from direct bromination of methylpyrazine by NBS. Since this compound is not so stable, the crude product after purification through a short silica-gel column was immediately used for the next reaction. The pyrazine derivative having the longest arm is prepared by insertion of an ether linkage in the alkyl chain because of the difficult availability of the corresponding pure alkyl compound. All central porphyrins, $\mathbf{P}^1$, $\mathbf{P}^5$, $\mathbf{P}^9$, $\mathbf{P}^{17}$, and $\mathbf{P}^{30}$, used in this work were prepared by the coupling reaction of *meso*-tetrakis(*p*-hydroxyphenyl)porphyrin with the corresponding bromoalkylpyrazine, which was catalysed by 18-crown-6. Although the yield of $\mathbf{P}^1$ was extremely low, probably due to the low purity of 2-bromomethylpyrazine, further synthetic refinement was not attempted. The electronic and fluorescence spectra of these porphyrins are essentially identical and no special interaction between the porphyrin core and pyrazinyl moieties was observed. The HRMS and NMR spectra of all final compounds show satisfactory agreement with the expected structures.

DOI: 10.1039/b408023h

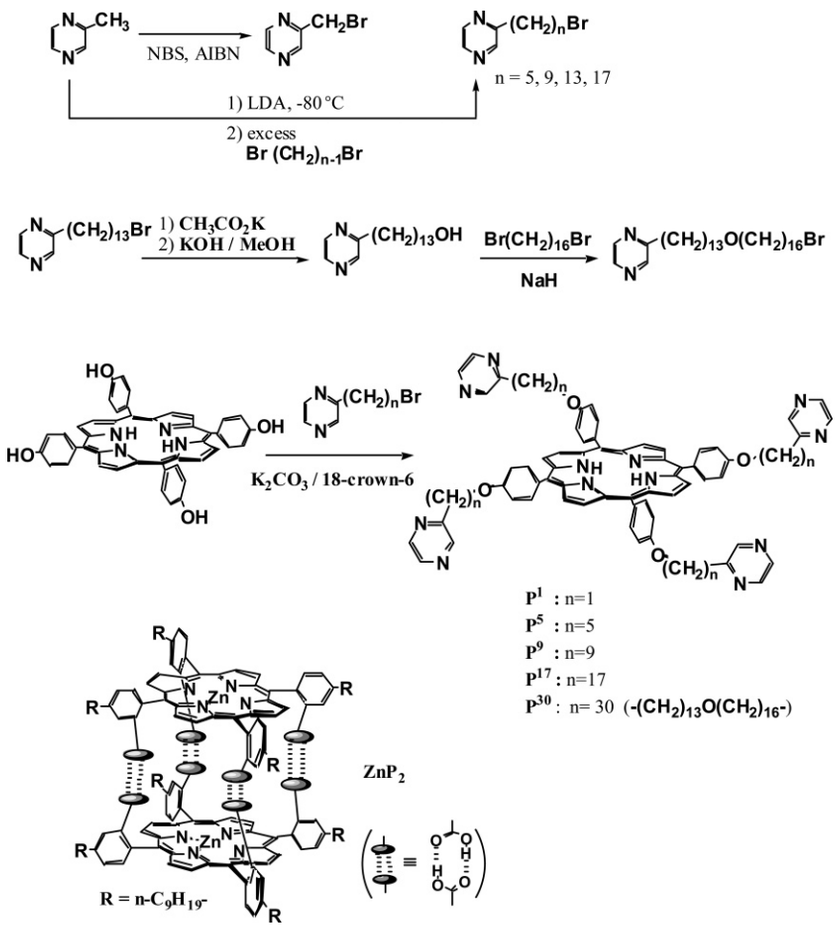

Scheme 1

Formation of nonameric porphyrin assemblies

The electronic spectra of $\mathbf{P^5}$, $\mathbf{ZnP_2}$ and the $\mathbf{ZnP_2}$·pyrazine complex are shown in Fig. 1. All electronic spectra of $\mathbf{P^5}$, $\mathbf{P^9}$, $\mathbf{P^{17}}$ and $\mathbf{P^{30}}$ are practically superimposable, which indicates that the appended pyrazine moieties do not perturb the spectra of the core TPP molecule, regardless of the length of the linker alkyl chains. The basic characteristics of the nonameric porphyrin assembly formation are examined by the spectroscopic titration experiments of dimeric [*meso*-tetrakis(2-carboxy-4-nonylphenyl)porphyrinato]zinc(II), $\mathbf{ZnP_2}$, with the free base porphyrins, $\mathbf{P^n}$. The typical result of the titration for the $\mathbf{ZnP_2}$–$\mathbf{P^5}$ system is shown in Fig. 2. Although there is no strict isosbestic point due to the absorbance of the titrant $\mathbf{P^5}$, its disturbance for the titration is fairly small because of the relatively low concentration of $\mathbf{P^5}$ during the experiment. The resulting spectroscopic behaviour is quite similar to that of the titration of $\mathbf{ZnP_2}$ with simple pyrazine derivatives reported previously.[5] The Q-band spectrum of the 4 : 1 mixture of $\mathbf{ZnP_2}$

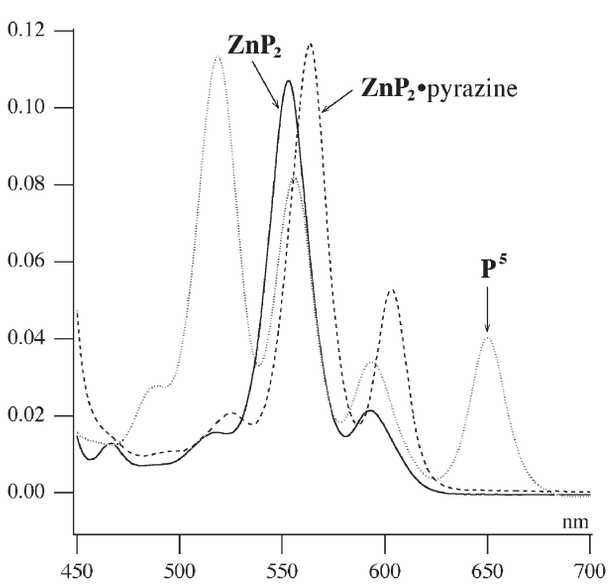

Fig. 1 Absorption spectra of $\mathbf{P^5}$ (8.09×10^{-6} M), $\mathbf{ZnP_2}$ (3.03×10^{-6} M) and $\mathbf{ZnP_2}$·pyrazine (3.01×10^{-6} M) in CH_2Cl_2.

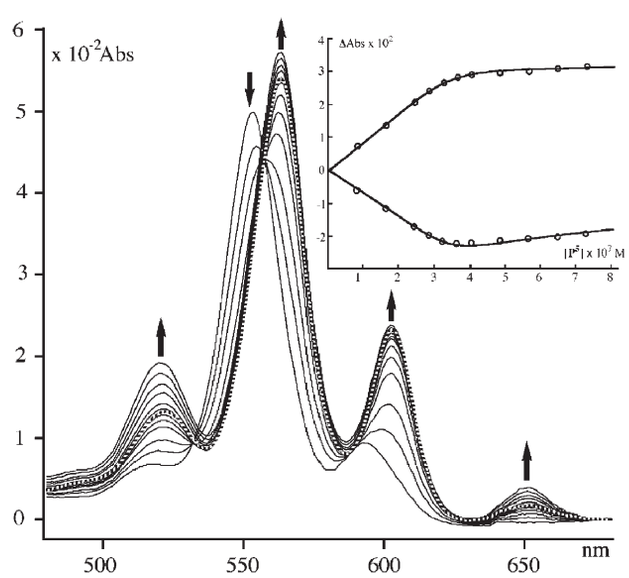

Fig. 2 UV/vis spectroscopic titration of $\mathbf{ZnP_2}$ with $\mathbf{P^5}$ in CH_2Cl_2: [$\mathbf{ZnP_2}$] = 1.41×10^{-6} M, [$\mathbf{P^5}$] = 0, 0.825, 1.64, 2.46, 2.86, 3.27, 3.67, 4.07, 4.87, 5.66, 6.45, 7.23×10^{-7} M. The dashed line is the composite spectrum of $\mathbf{ZnP_2}$·pyrazine (1.41×10^{-6} M) + $\mathbf{P^5}$ (3.52×10^{-7} M). The inset shows absorption changes at 549 and 566 nm: (○) observed points, (—) theoretical curves calculated by using eqn. (2) with $K = 9.2 \times 10^7$ M^{-1}.

and **P**[5] is practically identical with the composite spectrum of 4 × **ZnP**$_2$·pyrazine + **P**[5], *i.e.* both spectra show identical λ_{max} values within 0.5 nm errors and identical ε values over the whole Q-band region within 10% error.[7] Quite similar results are obtained for **P**[9], **P**[17] and **P**[30] assemblies. The stoichiometry of the assembly is also confirmed by Job's plot analysis shown in Fig. 3 in which **P**[17] is used as the central free base porphyrin. The maximum complex formation is observed at 0.88 of the molar fraction of monomeric **ZnP** which is consistent with 8/9 of the ideal value for the nonameric assembly. From these observations, we concluded that **P**[5], **P**[9], **P**[17] and **P**[30] form the 1 : 4 assemblies **P**[n]·(**ZnP**$_2$)$_4$, and that the electronic interaction between porphyrins in these assemblies is not sufficiently strong for it to seriously disturb the binding of **ZnP**$_2$ at each pyrazine site of **P**[n].[8] Thus the present assembling processes to form **P**[n]·(**ZnP**$_2$)$_4$ are reasonably expected to consist of four independent complexation processes of **ZnP**$_2$ at each pyrazine moiety of **P**[n], which have a practically identical binding constant and a site-independent molar absorptivity change during complexation of **ZnP**$_2$ (Scheme 2). Thus the process is analysed by using the theoretical model derived for the multiple equilibrium system that is statistically corrected for the identical multi-binding sites.[9]

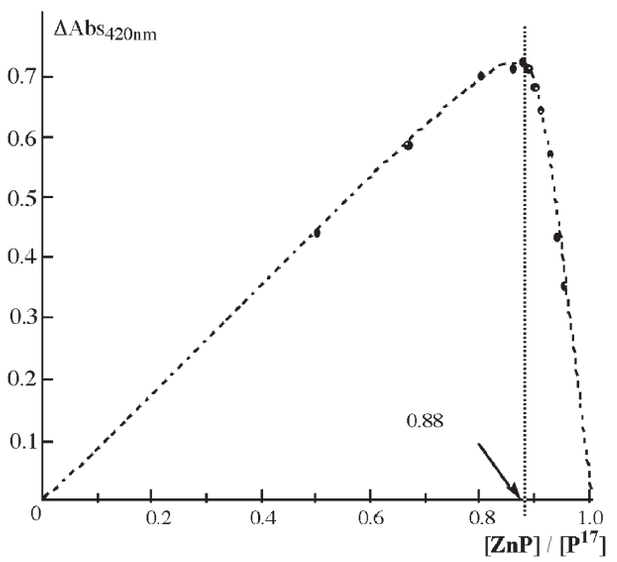

Fig. 3 The job's plot for the **ZnP**–**P**[17] system in CH_2Cl_2 at 298 K. The total porphyrin concentration is 2.63 × 10^{-6} M. Note that the ratio of the porphyrins is given in terms of the monomeric Zn porphyrin **ZnP**.

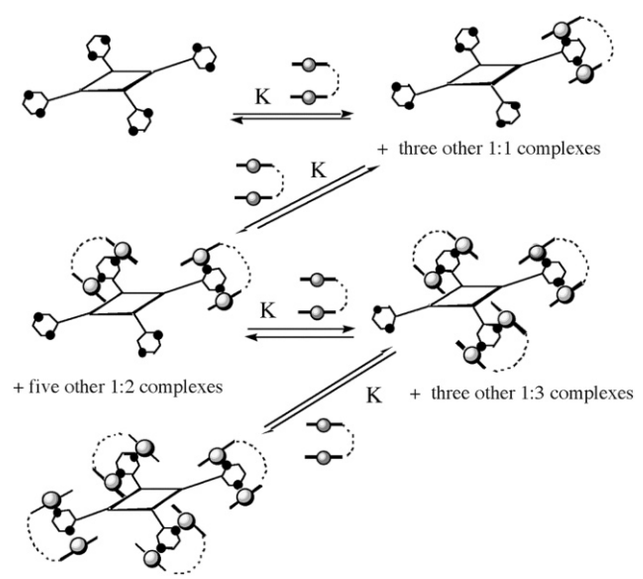

Scheme 2 Assembly formation equilibrium processes for four independent binding sites with an identical binding constant.

For the system having four identical binding sites, the binding constant K is defined by

$$K = \frac{[\mathbf{P}'' \bullet (\mathbf{ZnP}_2)_i]}{[\mathbf{ZnP}_2][\mathbf{P}'' \bullet (\mathbf{ZnP}_2)_{i-1}]} \quad i = 1,2,3,4. \tag{1}$$

Assuming the site-independent molar absorptivity ε_c for **ZnP**$_2$ complexing with the pyrazine moiety, the observed difference in absorption during the titration is expressed by

$$\begin{aligned} \mathrm{Abs} &= \mathrm{Abs}_{obs} - \varepsilon_{\mathbf{ZnP}_2}[\mathbf{ZnP}_2]_T \\ &= \frac{4K\Delta\varepsilon[\mathbf{ZnP}_2][\mathbf{P}'']_T}{1 + K[\mathbf{ZnP}_2]} + \varepsilon_{\mathbf{P}''}[\mathbf{P}'']_T \end{aligned} \tag{2}$$

where $\Delta\varepsilon$ is $\varepsilon_c - \varepsilon_{\mathbf{ZnP}_2}$ and the subscript T indicates the total concentration of the corresponding porphyrins. The observed data are in excellent agreement with eqn. (2) as shown in the inset of Fig. 2. All binding constants for **P**[5], **P**[9], **P**[17] and **P**[30] thus determined are of the order of 10^7 M^{-1},[10] which indicates that complex formation at these binding sites is very favourable and is insensitive to the distance from the central porphyrin and the apparent mutual proximity of the antenna porphyrins.

In contrast to these porphyrins having longer alkyl chains, **P**[1] shows somewhat different behaviour in the spectroscopic examination as shown in Fig. 4, *i.e.* the observed spectrum for **P**[1]·(**ZnP**$_2$)$_4$ is significantly different from that composed of the spectra of **P**[1] and the **ZnP**$_2$·pyrazine complex. The absorption band at 650 nm which is characteristic of **P**[1] clearly shifts to 655 nm upon complexation. Furthermore, the largest discrepancy is observed in the Soret region, where the **P**[1]·(**ZnP**$_2$)$_4$ complex shows a clear split of the main Soret absorption indicating that there are non-negligible electronic interactions between the component porphyrins in the assembly. These results suggest the possibility that the four independent binding site model shown in Scheme 2 is no longer proper for the **P**[1] assembly system. The experimental data for this system, however, are analysed by the same method applied for the other systems, since the titration curve still shows a monotonous single phase saturation and a sharp bend at the concentration ratio of **P**[1]/**ZnP**$_2$ = 1/4, similar to those for **P**[5] shown in Fig. 2. The resulting value of the binding constant for the **P**[1] system is *ca.* 1 × 10^7 M^{-1}, which shows that the binding of **P**[1] with **ZnP**$_2$ is still strong enough, although the binding constant should be considered as an apparent average value.

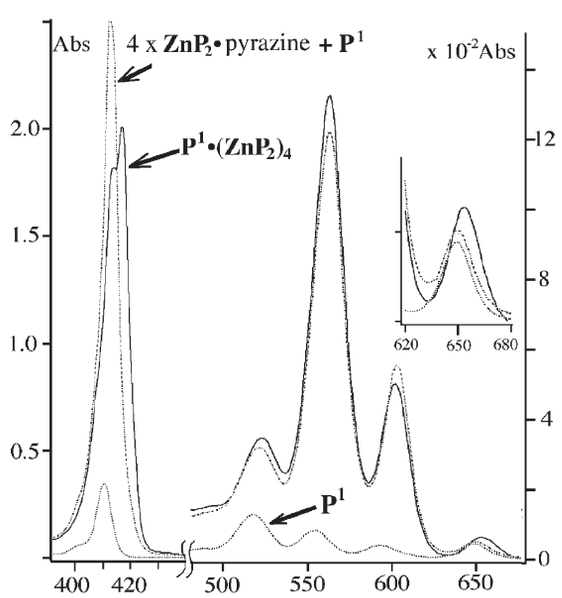

Fig. 4 Absorption spectra of **P**[1]·(**ZnP**$_2$) (7.56 × 10^{-7} M) and **P**[1] (7.56 × 10^{-7} M). The composite spectrum is reconstructed from the spectra of **ZnP**$_2$·pyrazine (3.02 × 10^{-6}M) + **P**[1] (7.56 × 10^{-7} M), where [**P**[1]] = 7.56 × 10^{-7} M.

Fluorescence spectroscopy and energy transfer reactions of the assemblies

The apparent antenna effects of the present assemblies are examined by fluorescence spectroscopy. The result of fluorescence titration of **ZnP**$_2$ with **P**^{9} is shown in Fig. 5. The system is excited at 564 nm where the largest Q-band absorption of the **ZnP**$_2$·pyrazine complex is observed. The basic behaviour is similar to that of the UV/vis titration. Upon addition of **P**^{9} to the solution of **ZnP**$_2$, the intensity of the fluorescence of **P**^{9} at 657 nm rapidly increases until the ratio of **P**^{9}/**ZnP**$_2$ = 1/4, where the titration curves plotted for the fluorescence intensity show a sharp saturation and further addition results in only a weak emission increase proportionate to the concentration of excess **P**^{9}. In contrast, the fluorescence of the **ZnP**$_2$·pyrazine moieties at 609 nm rapidly decreases until the ratio of **P**^{9}/**ZnP**$_2$ = 1/4. The observed emission under the saturation conditions is attributed mainly to the fluorescence of **P**^{9} despite the existence of a large excess of the **ZnP**$_2$·pyrazine moiety that is the main initial excitation species in the assembly. These observations indicate effective energy transfer from the **ZnP**$_2$ moieties to the central free base porphyrin **P**^{9} in the assembly and the intermolecular energy transfer is negligible under the present conditions. In order to quantitatively analyse the fluorescence behaviour of the present assembly, the spectra of the assembly and each component were compared in detail. The fluorescence spectra of **P**^{9}, the **ZnP**$_2$·pyrazine complex and the **P**^{9}·(**ZnP**$_2$)$_4$ assembly are shown in Fig. 6a. All spectra were measured at the standard conditions of [**P**^{9}] = 4.31 × 10^{-7} M and [**ZnP**$_2$] = 1.72 × 10^{-6} M. Since the spectrum observed for **P**^{9}·(**ZnP**$_2$)$_4$ still contains the fluorescence of the **ZnP**$_2$·pyrazine moiety, quantitative evaluation of this donor fluorescence intensity is expected to give good apparent indices for the intramolecular energy transfer in the assembly. The multiple regression analysis[11] for the observed emission of **P**^{9}·(**ZnP**$_2$)$_4$ reveals that the spectrum is well reconstructed by combination of the fluorescence F_1 for **P**^{9} and F_2 for the **ZnP**$_2$·pyrazine complex in the form of $f_aF_1 + f_bF_2$, where f_a and f_b are the amplifying factor for the acceptor emission and the quenching factor for the donor emission, respectively. The reconstructed spectrum shows excellent agreement with the observed fluorescence as shown in Fig. 6a. The fluorescence of free **ZnP**$_2$ is not detected in these analyses, indicating that practically all **ZnP**$_2$ molecules are bound to the pyrazine site of **P**^{n}. Similar results are also obtained for the **P**^{5}, **P**^{17} and **P**^{30} assemblies. These parameters thus determined are summarised in Table 1 together with the fluorescence quantum yields of the free base porphyrins and the absorption ratio of the donor and acceptor porphyrins in the assembly at 564 nm, r_{564},

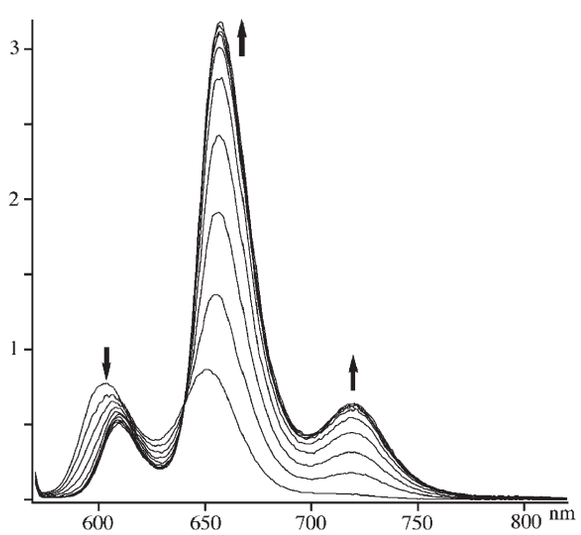

Fig. 5 Fluorescence spectroscopic titration of **ZnP**$_2$ with **P**^{9} in CH_2Cl_2 at 298 K. The assembly is excited at 564 nm; [**ZnP**$_2$] = 1.82 × 10^{-6} M, [**P**^{9}] = 0, 1.10, 2.17, 3.22, 3.99, 4.81, 5.58, 6.58, 7.56, 8.78 × 10^{-7} M.

Table 1 Fluorescence quantum yields of **P**^{n} and spectroscopic parameters of the assemblies **P**^{n}·(**ZnP**$_2$)$_4$[a]

Assembly	Φ[b]	r_{564}[c]	f_a[d]	f_b[e]
P^1	0.114	23	23	0.10
P^5	0.132	20	20	0.19
P^9	0.120	21	16	0.24
P^{17}	0.120	21	12	0.32
P^{30}	0.129	18	9	0.51

[a] In CH_2Cl_2, at 298 K. [b] The fluorescence quantum yield of **P**^{n}. The fluorescence quantum yields ϕ_F for **ZnP**$_2$ and **ZnP**$_2$·pyrazine were determined to be and 0.0294 and 0.0338, respectively. [c] The absorption ratio of **ZnP**$_2$·pyrazine and **P**^{n} in the assembly at 564 nm, evaluated from the spectrum reconstructed by calculation of 4 × **ZnP**$_2$·pyrazine + **P**^{n}. [d] The amplifying factor for the assembly (see text and Fig. 6a). [e] The fluorescence quenching factor for the **ZnP**$_2$·pyrazine fluorescence in the assembly.

which is an index of the initial amounts of the excited porphyrin components under the present conditions. As expected, the results indicate the general trend that the longer the alkyl chain length of **P**^{n}, the lower the apparent energy transfer efficiency, $(1-f_b)$, becomes. This point is discussed later in detail. The interesting relationship, $f_a \approx r_{564} \times (1-f_b)$, reported previously holds also for the present assemblies, indicating that the observed large enhancement of the fluorescence of **P**^{n} results directly from the absorption of the antenna pigments, **ZnP**$_2$.[4]

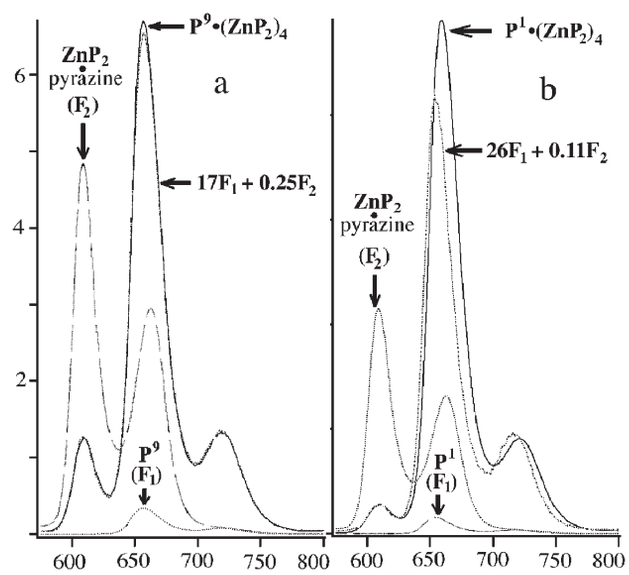

Fig. 6 Fluorescence spectra of the assemblies and their components in CH_2Cl_2 (λ_{ext} = 564 nm). a) The spectra of **P**^{9}·(**ZnP**$_2$)$_4$ (4.31 × 10^{-7} M), **P**^{9} (4.31 × 10^{-7} M) and **ZnP**$_2$·pyrazine (1.72 × 10^{-6} M). The composite spectrum is almost overlapping with the observed one. b) The spectra of **P**^{1}·(**ZnP**$_2$)$_4$ (7.25 × 10^{-7} M), **P**^{1} (7.25 × 10^{-7} M) and **ZnP**$_2$·pyrazine (2.90 × 10^{-6} M).

The emission spectra of the assembly constructed on **P**^{1} again show somewhat different behaviour. The fluorescence maxima of the assembly **P**^{1}·(**ZnP**$_2$)$_4$ at 660 and 722 nm are significantly different from those of uncomplexed **P**^{1} at 655 and 718 nm and, therefore, the notable discrepancy between the reconstructed spectrum and the observed one arises as shown in Fig. 6b. These observations clearly indicate that the electronic interaction between the central porphyrin of **P**^{1} and the antenna **ZnP**$_2$ moieties is not negligible in the assembly and that no simple relationships between absorption and emission may be expected for this smallest system. The quenching factor f_b obtained as the mathematical best fit value, however, may be still a fairly good index for the energy transfer in **P**^{1}(**ZnP**$_2$)$_4$, since the fluorescence component of **ZnP**$_2$·pyrazine at 609 nm seems to be unaffected by assembly formation.

Table 2 Fluorescence decay parameters for the porphyrin components[a]

Assembly	τ_0/ns[b]	k_f/ns^{-1}[c]
P[1]	7.81	0.0146
P[5]	8.54	0.0154
P[9]	8.36	0.0143
P[17]	8.46	0.0142
P[30]	8.20	0.0157
ZnP$_2$·pyrazine	3.20	0.0106
ZnP$_2$	3.03	0.0097

[a] In CH_2Cl_2, at 298 K. [b] The lifetime of the porphyrin fluorescence. [c] The rate constant for the radiative decay calculated from the relationship $k_f = \phi/\tau_0$, where ϕ is the fluorescence quantum yield given in Table 1.

Table 3 Kinetic parameters for the fluorescence decay process of the **ZnP**$_2$·pyarazine moieties in the assemblies[a]

Assembly	τ_1/ns[b]	k_{et}/ns^{-1}[c]	A_0[d]	A_1[d]
P[1]	0.107	9.03	0.020	0.116
P[5]	0.160	5.94	0.023	0.099
P[9]	0.474	1.80	0.017	0.052
P[17]	0.764	0.996	0.019	0.042
P[30]	1.26	0.484	0.019	0.031

[a] In CH_2Cl_2, at 298 K. [b] The lifetime for the faster component in the observed biphasic process. The slower lifetime τ_0 is fixed at 3.2 ns in all cases. [c] The rate constant of the intra-assembly energy transfer reaction calculated from $k_{et} = 1/\tau_1 - 1/\tau_0$. [d] The intensity factors for the slower and faster decay components of the fluorescence (see text).

Kinetic analyses of the energy transfer reaction in nonameric porphyrin assemblies

The dynamic aspects of the energy transfer reaction in the assemblies are investigated by the method of fluorescence lifetime analyses. At first, the lifetimes of the present porphyrin components were measured in dichloromethane. All observed decay profiles for these compounds show a clear, single exponential fluorescence decay and the resulting lifetimes are reasonable compared with the typical examples of those of TPP derivatives. The lifetimes of the component porphyrins used in this work are tabulated in Table 2 together with the rate constants of the radiative decay process, k_f, calculated from the lifetimes and the fluorescence quantum yields of the corresponding porphyrins. All lifetimes of central free base porphyrins are essentially identical, indicating that the photochemical dynamics of these porphyrins are unaffected by their alkylpyrazine moieties.

Based on the observed binding constants for the present assemblies, the concentration of the free **ZnP**$_2$ is expected to be negligibly low under the usual conditions of the assembly construction. Therefore, assuming the simple dynamic model as shown in Scheme 3a, the decay for the fluorescence from the excited antenna moiety, ^{A}**ZnP**$_2$*, in the 1 : 4 mixture of **P**^{n} and **ZnP**$_2$ is expected to show a single exponential curve, of which the rate may correspond to the sum of first order rate constants of the spontaneous decay, $k_n + k_f$, and the energy transfer process, k_{et}. A typical example of the fluorescence decay curve for the present assembly is shown in Fig. 7, where the fluorescence of the 1 : 4 mixture of **P**[9] and **ZnP**$_2$ is collected in the range from 590 to 620 nm where no fluorescence from **P**[9] appears. In spite of the above prediction, the observed decay is apparently biphasic. Since the decay curve is practically unaffected by addition of an excess of **P**[9], the additional decay process is not attributed to that of uncomplexed **ZnP**$_2$, though the slower lifetime component seems to be similar to that of **ZnP**$_2$·pyrazine. Similar biphasic behaviour is observed for all other assemblies used in the present work. The results strongly indicate that there are some energy transfer inactive **ZnP**$_2$·pyrazine moieties in the assembly, ^{A}**ZnP**$_2$$^\#$, which do not equilibrate with the active ones, ^{A}**ZnP**$_2$*, within the time range of the present photochemical processes (Scheme 3b). Thus, all fluorescence decay data were analysed by using the biphasic kinetic model,

$$F(t) = A_0\exp(-t/\tau_0) + A_1\exp(-t/\tau_1) \quad (3)$$

where F is fluorescence intensity, τ_0 and τ_1, are lifetimes and A_0 and A_1 are corresponding intensity factors for the fluorescence of ^{A}**ZnP**$_2$$^\#$ and ^{A}**ZnP**$_2$*, respectively. Since it is confirmed that the longer lifetime τ_0 is practically equal to that of the **ZnP**$_2$·pyrazine complex, 3.2 ns, in all cases the decay curve analyses were performed by optimising τ_1 using the fixed τ_0 value. The energy transfer rate constants k_{et} for the present assemblies are calculated from the standard equation, $k_{et} = 1/\tau_1 - 1/\tau_0$. The resulting τ_1, k_{et} and intensity factors A_0 and A_1 are summarised in Table 3.

Discussion

The present energy transfer reaction is expected to proceed *via* a through-space Förster mechanism. The most direct confirmation of the mechanism may be obtained from examination of the relationship between the energy transfer rate and the donor–acceptor distance. In order to examine this point, we have adopted two kinds of distance indices for the present porphyrin assemblies. The first index is a center-to-center separation distance (R_{et}) between the zinc porphyrin and the free base porphyrin estimated from the Förster equation,[12]

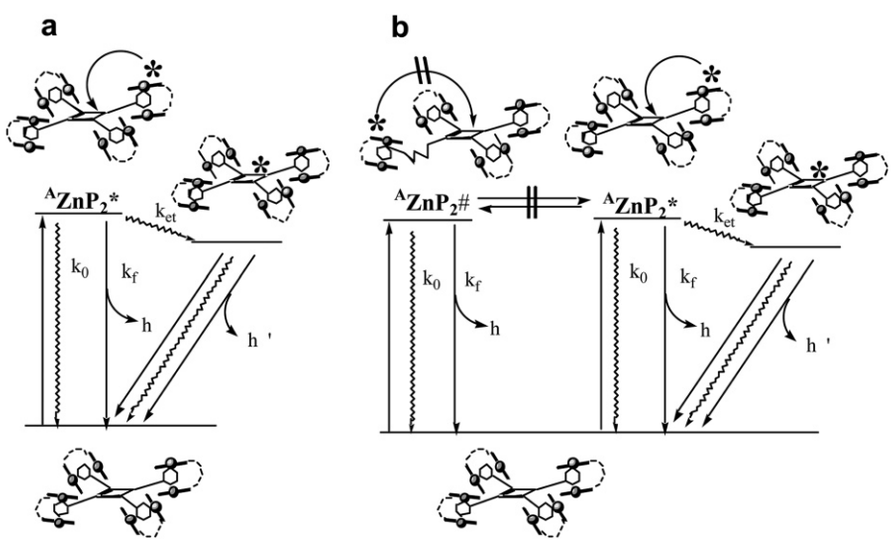

Scheme 3 Photochemical processes for the porphyrin assembly: a) the single kinetic cycle model containing a energy transfer path from homogeneous antenna porphyrins ^{A}**ZnP**$_2$*: b) the parallel kinetic model containing energy transfer inactive antenna porphyrin ^{A}**ZnP**$_2$$^\#$.

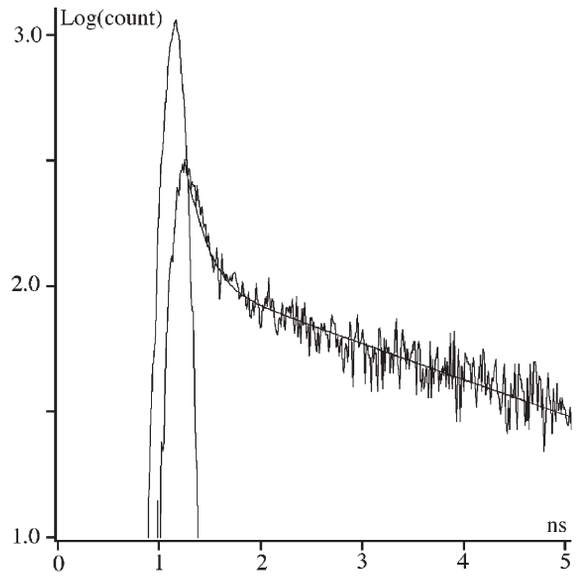

Fig. 7 Fluorescence decay profile of $\mathbf{P}^{5}\cdot(\mathbf{ZnP}_2)_4$ in CH_2Cl_2 collected in the 590–620 nm range. The sample is excited at 406 nm. The solid line is calculated by $F(t) = 0.023\exp(-t/3.2) + 0.16\exp(-t/0.16)$.

$$k_{et} = \frac{(8.8\times10^{-25})\kappa^2\phi_f J_F}{n^4\tau_0 R_{et}^6} \quad (4)$$

where κ is an orientation factor ($\kappa = 2/3$ for random orientation),[13] ϕ_f is the fluorescence quantum yield of the donor given in the caption of Table 1, n is the solvent refractive index and J_F is the overlap integral obtained from the fluorescence intensity at wavenumber ν ($F(\nu)$) of the donor and the molar extinction coefficient ($\varepsilon(\nu)$) of the Q_y absorption band of the acceptor in the following form,

$$J_F = \frac{\int F(\nu)\varepsilon(\nu)\nu^{-4}\mathrm{d}\nu}{\int F(\nu)\mathrm{d}\nu} \quad (5)$$

The second distance index is the following end-to-end distance L, statistically calculated for the free alkyl chain $(CH_2)_{m+1}$,

$$<L^2> = ml^2\left\{\frac{1+\lambda}{1-\lambda} - \frac{2\lambda(1-\lambda^m)}{m(1-\lambda)^2}\right\} \quad (6)$$

where $<L^2>$ is the average square end-to-end distance, m is the number of the bond, l is the bond length of the C–C unit and λ is $\cos(\pi-\theta)$ for the bond angle θ of the alkyl chain.[14] The actual center-to-center distance between the donor and the acceptor (R_{st}) statistically estimated is calculated by adding the fixed length of the rigid aromatic part of the structures to L as shown in the Fig. 8. The values of R_{et} and R_{st} are summarised in Table 4. There is excellent agreement between R_{et} and R_{st} in spite of quite

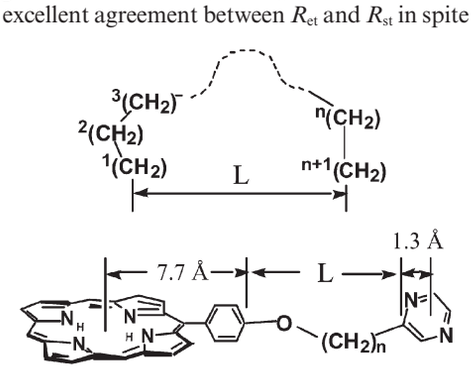

$R_{st} = 7.7 + L + 1.3$

Fig. 8 Statistical center-to-center distance, R_{st}, between the donor and the acceptor connected with the alkyl chain $(CH_2)_{n+1}$.

Table 4 Center-to-center distances (Å) estimated from the Förster equation [eqn. (4)] and the statistical conformation analysis for the free alkyl chains

Assembly	R_{et} [a]	R_{st} [b]
$\mathbf{P}^1$	12.8	12.3
$\mathbf{P}^5$	13.7	14.4
$\mathbf{P}^9$	16.8	16.0
$\mathbf{P}^{17}$	18.5	18.3
$\mathbf{P}^{30}$	20.8	21.2

[a] The distance estimated from Förster's equation (see text). [b] The distance estimated by using the statistical length of alkyl chains (see Fig. 8).

different origins of these two distance indices and apparently rough simplification for estimation of R_{st}. The results are also confirmed more clearly by the logarithmic plot of k_{et} *vs.* R_{st} shown in Fig. 9. The observed linear relationship with the slope of −6 indicates that the present intra-assembly energy transfer reactions may mainly proceed *via* the Förster mechanism.[15]

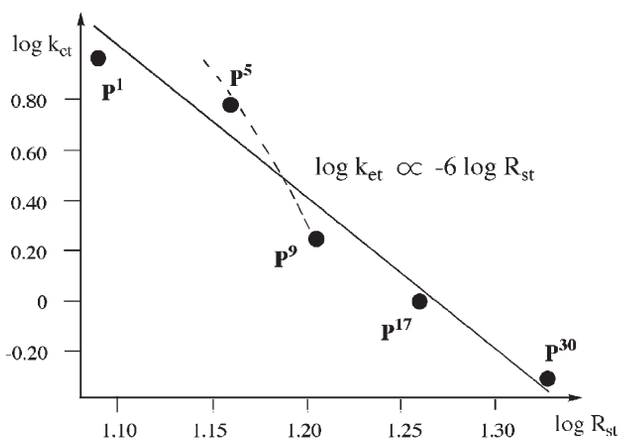

Fig. 9 Logarithmic plot of R_{st} *vs.* k_{et}. The slope of the straight line is −6. The dashed line shows one possible curve calculated for the Dexter mechanism using a Bohr radius of *ca.* 3 Å. See discussion in ref. 15.

Since fairly wide range for the energy transfer rate is observed in the present systematic assembly series, it may be interesting to inspect the quantitative relationship between the data of the steady-state fluorescence spectroscopy and the dynamic one. The energy transfer efficiency evaluated from the fluorescence spectroscopy, ${}^{ss}\phi_{et} = 1-f_b$, and that from the kinetic measurement, ${}^{dy}\phi_{et} = k_{et}/(k_o+k_f+k_{et})$, are tabulated in Table 4. The discrepancy between these two values found in all assemblies evidently comes from the fact that the efficiency ${}^{dy}\phi_{et}$ does not take into account the effect of the energy transfer inactive antenna porphyrin ${}^{A}\mathbf{ZnP}_2{}^{\#}$. The total energy transfer efficiency ${}^{T}\phi_{et}$ may be evaluated by using the intensity factors A_0 and A_1, which contain the initial concentration and the fluorescence quantum yields for ${}^{A}\mathbf{ZnP}_2{}^{\#}$ and ${}^{A}\mathbf{ZnP}_2{}^{*}$, $\phi_0 = k_f/(k_0+k_f)$ and $\phi_1 = k_f/(k_0+k_f+k_{et})$ as follows,

$$\frac{A_0}{A_1} = \frac{\phi_0[{}^{A}\mathbf{ZnP}_2^{\#}]_{init}}{\phi_1[{}^{A}\mathbf{ZnP}_2^{*}]_{init}}. \quad (7)$$

The total energy transfer efficiency ${}^{T}\phi_{et}$ is obtained by using the intensity ratio,

$${}^{T}\phi_{et} = 1 - \frac{{}^{T}\phi_f}{\phi_0} = \frac{\phi_0-\phi_1}{(A_0/A_1)\phi_1+\phi_0} \quad (8)$$

where ${}^{T}\phi_f$ is the following total fluorescence quantum yield for the present assembly:

$${}^{T}\phi_f = \frac{\phi_0[{}^{A}\mathbf{ZnP}_2^{\#}]_{init}+\phi_1[{}^{A}\mathbf{ZnP}_2^{\#}]_{init}}{[{}^{A}\mathbf{ZnP}_2^{\#}]_{init}+[{}^{A}\mathbf{ZnP}_2^{\#}]_{init}} = \frac{(1+A_0/A_1)\phi_1\phi_0}{(A_0/A_1)\phi_1+\phi_0} \quad (9)$$

Table 5 Comparison of the apparent and calculated energy transfer efficiencies

Assembly	$^{ss}\phi_{et}$ [a]	$^{dy}\phi_{et}$ [b]	$^{T}\phi_{et}$ [c]
P[1]	0.90	0.96	0.96
P[5]	0.81	0.95	0.93
P[9]	0.76	0.85	0.81
P[17]	0.68	0.76	0.68
P[30]	0.49	0.61	0.48

[a] The efficiency obtained from the steady-state fluorescence spectroscopic data ($1-f_b$). [b] The apparent efficiency calculated from the energy transfer rate constant, $k_{et}/(k_0+k_f+k_{et})$. [c] The efficiency corrected for the effect of energy transfer inactive ^{A}**ZnP**$_2^{\#}$ (see text).

The values of $^{T}\phi_{et}$ calculated by using ϕ_0 observed for the **ZnP**$_2$·pyrazine complex and ϕ_1 evaluated from the kinetic data for ^{A}**ZnP**$_2$* are also tabulated in Table 5. The values of $^{T}\phi_{et}$ thus obtained show reasonable agreement with those obtained by the steady-state fluorescence measurement. In this evaluation, it is also interesting to note that the energy transfer active antenna moiety ^{A}**ZnP**$_2$* is always the main antenna component in all of the assemblies, though ^{A}**ZnP**$_2^{\#}$ seems to a play more significant role in the larger assemblies, *i.e.* the relative amounts of ^{A}**ZnP**$_2^{\#}$ estimated from eqn. (7) are *ca.* 0.6, 1, 5, 10 and 24% for **P**[1], **P**[5], **P**[9], **P**[17] and **P**[30], respectively. The observation that the relative amount of ^{A}**ZnP**$_2^{\#}$ seems to be depend upon the spatial scale of the assembly and not upon the number of the antenna porphyrins suggests that the observed non-homogeneity of the antenna moieties has its origin in the size of the degree of conformational freedom of the assembly.

Conclusion

The present assembly systems show a significant antenna effect, light-condensation and intensification of the excited state of the specific central porphyrin. The process of the intra-assembly energy transfer reaction is shown to proceed *via* a typical Förster mechanism. The advantage of the self-assembling methodology is clear not only from the viewpoint of the fact that the systematic series of porphyrin assemblies are easily obtained, but also from the fact that the physical properties of the partial structure in each assembly is easily evaluated by using the corresponding separated component.

The investigation of the dynamic aspects of the assemblies unexpectedly reveals that the antenna porphyrins in the assemblies are not in a homogeneous state. Although the actual structural properties of the energy transfer inactive antenna site ^{A}**ZnP**$_2$* are unknown, it is interesting to note that the dendritic multi-porphyrin system also shows similar multi-phasic fluorescence decay behaviour.[16] In order to identify the exact state of ^{A}**ZnP**$_2^{\#}$, more detailed analyses of the fast spectroscopic data, such as consideration of the multi-phase photochemical process not only for the antenna moiety but also for the acceptor porphyrin **P**[n], will be necessary.

Another interesting application of the present multi-porphyrin assembly is the introduction of a built-in charge separation system that contains an appropriate electron acceptor moiety. These developmental investigations are now underway in our laboratory.

Experimental

^{1}H-NMR spectra were recorded on a Varian Gemini 200 (200 MHz) or a Brucker ARX500 (500 MHz) spectrometer in deuteriochloroform or deuteriotetrahydrofuran using the residual solvent peaks as internal standards of chemical shift. Low resolution mass spectra were obtained by using SHIMADZU QP-5000 (EI) or BRUKER REFLEX III (MALDI-TOF) instruments. High resolution mass spectra (HRMS) were recorded on a JEOL-700 (FAB) spectrometer. Electronic absorption spectra were obtained by using SHIMADZU Multispec-1500 multichannel Photodiode Array Spectrometer with a Toshiba UV-35 cut-off filter. Fluorescence spectra were recorded on a HITACHI F-4500 spectrofluorometer. The time-resolved fluorescence lifetime measurements were performed using a Hamamatsu Photonics C-4780 instrument with a picosecond light pulser PLP-10 at 406 nm. Samples for the fluorescence lifetime measurements were used after nitrogen gas bubbling. *meso*-Tetrakis(2-carboxy-4-nonylphenyl)porphyrin and its zinc complex (**ZnP**) were prepared according to our previously reported methods.[5]

2-(5-Bromopentyl)pyrazine

To a solution of diisopropylamine (1.61 g, 15.9 mmol) in THF (10 ml) was added dropwise 1.6 M *n*-BuLi in hexane (10 ml, 15.9 mmol) at −78 °C, with stirring for 1.5 h at this temperature. 2-Methylpyrazine (1.02 g, 10.8 mmol) in THF (5 ml) was added into the solution at −78 °C. The reddish-purple mixture was maintained for 3 h at −78 °C with stirring, and then 1,4-dibromobutane (4.59 g, 21.3 mmol) in THF (5 ml) was added. The reaction mixture was allowed to warm gradually to room temperature, and stirring at this temperature was continued for 16 h. The reaction was quenched by addition of an excess amount of solid NH_4Cl, and the mixture was filtered and concentrated under reduced pressure. The residue was purified by column chromatography on silica-gel eluted by hexane to hexane/ether = 1/1 to afford 1.28 g (5.59 mmol, 53%) of a colorless oil. ^{1}H-NMR (200 MHz, $CDCl_3$): δ 8.49 (dd, 1H, J = 1.4, 2.4 Hz, 5-pyrz–H), 8.46 (d, 1H, J = 1.4 Hz, 3-pyrz–H), 8.40 (d, 1H, J = 2.4 Hz, 6-pyrz–H), 3.41 (t, 2H, J = 6.8 Hz, –OCH_2–), 2.83 (t, 2H, J = 7.6 Hz, pyrz–CH_2–), 2.00–1.70 (m, 4H, –OCH_2–CH_2– and pyrz–CH_2–CH_2–), 1.62–1.42 (m, 2H, –CH_2–).

2-(9-Bromononyl)pyrazine

52% (colorless oil). ^{1}H-NMR (200 MHz, $CDCl_3$): δ 8.48 (dd, 1H, J = 1.6, 2.4 Hz 5-pyrz–H), 8.45 (d, 1H, J = 1.6 Hz 3-pyrz–H), 8.38 (d, 1H, J = 2.4 Hz, 6-pyrz–H,), 3.39 (t, 2H, J = 7.1 Hz, –OCH_2–), 2.80 (t, 2H, J = 7.7 Hz, pyrz–CH_2–), 1.92–1.64 (m, 4H, –OCH_2–CH_2–, pyrz–CH_2–CH_2–), 1.50–1.16 [m, 10H, –$(CH_2)_5$–]. MS (EI): m/z 284, 286 $[M]^+$.

2-(13-Bromotridecanyl)pyrazine

60% (colorless oil). ^{1}H-NMR (200 MHz, $CDCl_3$): δ 8.48–8.45 (m, 2H 3 and 5-pyrz–H), 8.40 (d, 1H, J = 2.4 Hz, 6-pyrz–H,), 3.41 (t, 2H, J = 6.6 Hz, –OCH_2–), 2.81 (t, 2H, J = 7.3 Hz, pyrz–CH_2–), 1.94–1.65 (m, 4H, –OCH_2–CH_2–, pyrz–CH_2–CH_2–), 1.48–1.15 [m, 18H, –$(CH_2)_5$–]. MS (EI): m/z 340, 342 $[M]^+$.

2-(17-Bromoheptadecanyl)pyrazine

29% (colorless oil). ^{1}H-NMR (200 MHz, $CDCl_3$): δ 8.49 (dd, 1H, J = 1.3, 2.4 Hz, 5-pyrz–H), 8.46 (d, 1H, J = 1.3 Hz, 3-pyrz–H), 8.39 (d, 1H, J = 2.4 Hz, 6-pyrz–H), 3.41 (t, 2H, J = 6.9 Hz, $BrCH_2$–), 2.62 (t, 2H, J = 8.3 Hz, pyrz–CH_2–), 2.02–1.51 (m, 4H, $BrCH_2$–CH_2–, pyrz–CH_2–CH_2–), 1.44–0.79 [m, 26H, –$(CH_2)_{13}$–].

2-(13-Hydroxyltridecananyl)pyrazine

A mixture of 2-(13-bromotridecanyl)pyrazine (0.27 g, 0.8 mmol) and potassium acetate (0.8 g, 8.2 mmol) in DMF (11 ml) was stired for 2 h at 60 °C under nitrogen. After evaporation of the solvent under reduced pressure the residue was treated with KOH (500 mg) in methanol (13 ml) at 60 °C. The mixture was concentrated, and extracted with dichloromethane. The extract was washed twice by water, and dried over sodium sulfate. Evaporation of the solvent gave almost pure product (0.19 g, 92%) which was used without further purification. ^{1}H-NMR (200 MHz, CDCl3): δ 8.63–8.36 (m, 3H, pyrz–H), 3.62 (t, 2H, J = 6.7, –CH_2–O), 2.83 (t, 2H, J = 7.9, –CH_2–pyrz), 1.86–1.66

(m, 2H, –O–$CH_2C\mathit{H}_2$–), 1.64–1.45 (m, 2H, pyrz–$CH_2C\mathit{H}_2$–), 1.40 (m, 18H, other –CH_2–).

2-(30-Bromo-17-oxatricontane)pyrazine

2-(13-Hydroxyltridecananyl)pyrazine (133 mg, 0.48 mmol) dissolved in THF (5 ml) was treated with NaH (60%, 100 mg) under nitrogen, and was reacted with 1,16-dibromohexadecane (371 mg, 0.97 mmol) in THF (3 ml) under reflux for 16 h. The reaction mixture was quenched by methanol, and concentrated under reduced pressure. The residue was dissolved in dichloromethane, washed with water, and dried over sodium sulfate. The crude products were purified by silica-gel chromatography eluted with hexane–diethyl ether (100/0 to 40/60) to afford 122 mg (45%) of product. ^{1}H-NMR (200 MHz, $CDCl_3$): δ 8.5–8.4 (m, 3H, pyrz–H), 3.5–3.3 (m, 6H, Br–CH_2–, –CH_2–O–CH_2), 2.82 (t, 2H, J = 7.8 Hz, pyrz–CH_2–), 1.86–1.11 (m, 48H, CH_2).

2-(Bromomethyl)pyrazine

A solution of *N*-bromosuccinimide (3.78 g, 21.2 mmol), AIBN (3.43 g, 20.9 mmol), and 2-methylpyrazine (2.00 g, 21.2 mmol) in benzene (15 ml) was refluxed for 1 h. After cooling in an ice-bath, the mixture was filtered, and the solvent was evaporated under reduced pressure. The residue was chromatographed on silica-gel eluted with hexane/diethyl ether to afford almost pure product, which was immediately used for the next porphyrin synthesis since it was unstable at room temperature under air. ^{1}H-NMR (200 MHz, $CDCl_3$): δ 8.71 (d, 1H, J = 1.4 Hz, 3-pyrz–H), 8.54 (dd, 1H, J = 1.4, 2.5 Hz, 5-pyrz–H), 8.49 (d, 1H, J = 2.5 Hz, 6-pyrz–H), 4.55 (s, 2H, –CH_2–). MS (EI): m/z 172, 174 $[M]^+$.

Tetrakis[*p*-{5-(2-pyrazinyl)-*n*-pentoxy}phenyl]porphyrin (P^5)

A mixture of tetrakis(*p*-hydroxyphenyl)porphyrin (113.5 mg, 0.167 mmol), 2-(5-bromo-*n*-pentyl)pyrazine (475.8 mg, 2.08 mmol), K_2CO_3 (476.1 mg, 3.44 mmol), and 18-crown-6 (93.4 mg, 0.353 mmol) in DMF (10 ml) was stirred at 60 °C under N_2 overnight. The reaction mixture was cooled to room temperature, and the solvent was evaporated under reduced pressure. The residue was dissolved in CH_2Cl_2, washed with water, and dried over sodium sulfate. Filtration, followed by evaporation of the solvent gave a crude product as a black solid which was twice purified by column chromatography on silica-gel eluted with CH_2Cl_2/MeOH (100/0 to 95/5), and recrystallized from CH_2Cl_2/MeOH to afford 108 mg (0.085 mmol, 51%). ^{1}H-NMR (500 MHz, $CDCl_3$): δ 8.83 (s, 8H, pyrrole), 8.53–8.51 (m, 8H, 3 and 5-pyrz–H), 8.42 (d, 4H, J = 2.3 Hz, 6-pyrz–H), 8.08 (d, 8H, J = 8.1 Hz, 2-Ph–H) 7.24 (d, 8H, J = 8.1 Hz, 1-Ph–H), 4.25 (t, 8H, J = 6.0 Hz, Ph–OCH_2–), 2.52 (t, 8H, J = 7.9 Hz, pyrz–CH_2–), 2.06–1.99 (m, 8H, PhOCH_2–$C\mathit{H}_2$–), 1.99–1.91 (m, 8H, PyCH_2–$C\mathit{H}_2$–), 1.79–1.68 (m, 8H, –CH_2–$C\mathit{H}_2$–CH_2–), −2.77 (brs, 2H, inner N–H); HRMS (FAB): m/z 1270.6283 $[M]^+$. Calc. for $C_{80}H_{78}O_4N_{12}$: 1270.6269 (Δ = +1.1 ppm). UV-Vis (CH_2Cl_2): λ_{max}/nm (logε) 422 (5.62), 519 (4.15), 556 (4.01), 595 (3.64), 651 (3.70).

Tetrakis{*p*-(2-pyrazinyl)methoxyphenyl}porphyrin (P^1)

9%. ^{1}H-NMR (500 MHz, $CDCl_3$): δ 9.06 (d, 4H, J = 1.5 Hz, 3-pyrz–H), 8.84 (s, 8H, pyrrole–H), 8.66 (dd, 4H, J = 1.5, 2.4 Hz, 5-pyrz–H), 8.63 (d, 4H, J = 2.4 Hz, 6-pyrz–H), 8.14 (d, 8H, J = 8.2 Hz, Ph–H), 7.38 (d, 8H, J = 8.2 Hz, Ph–H), 5.33 (s, 8H, –CH_2–), −2.79 (brs, 2H, inner N–H). HRMS (FAB): m/z 1046.3771 $[M]^+$. Calc. for $C_{64}H_{46}O_4N_{12}$: 1046.3765 (Δ = +0.6 ppm). UV-Vis (CH_2Cl_2): λ_{max}/nm (logε) 421 (5.66), 518 (4.21), 554 (4.02), 595 (3.69), 650 (3.74).

Tetrakis[*p*-{9-(2-pyrazinyl)-*n*-nonoxy}phenyl]porphyrin (P^9)

13%. ^{1}H-NMR (500 MHz, $CDCl_3$): δ 8.84 (s, 8H, pyrrole–H), 8.48 (dd, 4H, J = 1.6, 2.5 Hz, 5-pyrz–H), 8.46 (d, 4H, J = 1.6 Hz, 3-pyrz–H), 8.37 (d, 4H, J = 2.5 Hz, 6-pyrz–H), 8.08 (d, 8H, J = 8.6 Hz, 2-Ph–H) 7.25 (d, 8H, J = 8.6 Hz, 1-Ph–H), 4.23 (t, 8H, J = 6.6 Hz, Ph–OCH_2–), 2.83 (t, 8H, J = 7.6 Hz, pyrz–CH_2–), 1.99–1.93 (m, 8H, PhOCH_2–$C\mathit{H}_2$–), 1.82–1.74 (m, 8H, pyrz–CH_2–$C\mathit{H}_2$–), 1.64–1.57 [m, 8H, PhO$(CH_2)_2$–$C\mathit{H}_2$–], 1.49–1.38 [m, 32H, –CH_2–$(C\mathit{H}_2)_4$–CH_2–], −2.76 (brs, 2H, inner N–H). HRMS (FAB): m/z 1494.8776 $[M]^+$. Calc. for $C_{96}H_{110}O_4N_{12}$: 1494.8773 (Δ = +0.2 ppm). UV-Vis (CH_2Cl_2): λ_{max}/nm (logε) 422 (5.54), 519 (4.10), 556 (3.97), 595 (3.59), 651 (3.67).

Tetrakis[*p*-{17-(2-pyrazinyl)-*n*-heptadecanoxy}phenyl]porphyrin (P^{17})

29%. ^{1}H-NMR (500 MHz, $CDCl_3$): δ 8.84 (s, 8H, pyrrole–H), 8.45 (dd, 4H, J = 1.4, 2.5 Hz, 5-pyrz–H), 8.42 (d, 4H, J = 1.4 Hz, 3-pyrz–H), 8.35 (d, 4H, J = 2.5 Hz, 6-pyrz–H), 8.09 (d, 8H, J = 8.5 Hz, 2-Ph–H), 7.26 (d, 8H, J = 8.5 Hz, 1-Ph–H), 4.23 (t, 8H, J = 6.5 Hz, Ph–OCH_2–), 2.77 (t, 8H, J = 7.8 Hz, pyrz–CH_2–), 2.00–1.93 (m, 8H, PhOCH_2–$C\mathit{H}_2$–), 1.75–1.68 (m, 8H, pyrz–CH_2–$C\mathit{H}_2$–), 1.64–1.55 (m, 8H, –CH_2–$C\mathit{H}_2$–CH_2–), 1.49–1.42 (m, 8H, –CH_2–$C\mathit{H}_2$–CH_2–), 1.42–1.23 [m, 88H, –$(CH_2)_{11}$–], −2.77 (brs, 2H, inner N–H); HRMS (FAB): m/z 1943.3735 $[M]^+$. Calc. for $C_{128}H_{174}O_4N_{12}$: 1943.3781 (Δ = −2.4 ppm). UV-Vis (CH_2Cl_2) λ_{max}/nm (logε) 422 (5.54), 519 (4.11), 557 (3.98), 595 (3.60), 652 (3.76).

Tetrakis[*p*-{30-(2-pyrazinyl)-17-oxatricontanoxy}phenyl]-porphyrin (P^{30})

Preparative HPLC (ODS) eluted with methanol followed by recrystallization from dichloromethane/methanol gave 3.4 mg (3%) product. ^{1}H-NMR (500 MHz, CD_2Cl_2): δ 8.93 (s, 8H, pyrrole–H), 8.46 (dd, 4H, J = 1.5, 2.5 Hz, 5-pyrz–H), 8.44 (d, 4H, J = 1.5 Hz, 3-pyrz–H), 8.36 (d, 4H, J = 2.5 Hz, 6-pyrz–H), 8.14 (d, 8H, J = 6.5 Hz, 2-Ph–H), 7.33 (d, 8H, J = 6.5 Hz, 1-Ph–H), 4.30 (t, 8H, J = 6.5 Hz, Ph–OCH_2–), 3.39–3.37 (m, 16H, –CH_2–OCH_2–), 2.80 (t, 8H, J = 7.8 Hz, pyrz–CH_2–), 2.05–1.99 (m, 8H, PhOCH_2–$C\mathit{H}_2$–), 1.77–1.71 (m, 8H, pyrz–CH_2–$C\mathit{H}_2$–), 1.70–1.64 (m, 8H, –CH_2–$C\mathit{H}_2$–CH_2–), 1.58–1.23 (m, 176H, other –CH_2–), −2.77 (brs, 2H, inner N–H); HRMS (FAB): m/z 2680.1079 $[M]^+$. Calc. for $C_{176}H_{270}O_8N_{12}$: 2680.1090 (Δ = −0.4 ppm). UV-Vis (CH_2Cl_2) λ_{max}/nm (logε) 422 (5.60), 519 (4.16), 557 (4.04), 595 (3.67), 652 (3.77).

References

1 J. Deisenhofer, O. Epp, K. Miki, R. Huber and H. Michel, *Nature*, 1985, **318**, 618; G. McDermott, S. M. Prince, A. A. Freer, A. M. Hawthornthwaite-Lawless, M. Z. Papiz, R. J. Cogdell and N. W. Isaacs, *Nature*, 1995, **374**, 517; T. Pullerits and V. Sundstrom, *Acc. Chem. Res.*, 1996, **29**, 381.

2 For examples of recent developments, see: M. Wasielewski, *Chem. Rev.*, 1992, **92**, 435; D. Gust, T. A. Moore and A. L. Moore, *Acc. Chem. Res.*, 1993, **26**, 198; H. Kurreck and M. Fuber, *Angew. Chem., Int. Ed. Engl.*, 1995, **34**, 849; A. Harriman and J.-P. Sauvage, *Chem. Soc. Rev.*, 1996, **24**, 41; V. Balzani, A. Juris, M. Venturi, S. Champagna and S. Serroni, *Chem. Rev.*, 1996, **96**, 759; M.-J. Blanco, M. C. Jiménez, J.-C. Chambron, V. Heitz, M. Linke and J.-P. Sauvage, *Chem. Soc. Rev.*, 1999, **28**, 293; D. Gust, T. A. Moore and A. L. Moore, *Acc. Chem. Res.*, 2001, **34**, 40; M.d. R. Benitetes, T. E. Johnson, S. Weghorn, L. Yu, P. D. Rao, J. R. Diers, S. I. Yang, C. Kimaier, D. F. Bocian, D. Holte and J. S. Lindsey, *J. Mater. Chem.*, 2002, **12**, 65; V. Balzani, A. Credi, M. Venturi, *Molecular Devices and Machines – A Journey into the Nano World*, Wiley-VCH Verlag GmbH & Co. KGaA, Weinheim, 2003.

3 For recent reviews of the porphyrin assemblies, see: H. Ogoshi, T. Mizutani, T. Hayashi and Y. Kuroda, in *The Porphyrin Handbook. Vol.6, Applications: Past, Present and Future*, K. M. Kadish, K. M. Smith and R. Guilard, ed., Academic Press, New York, 2000, pp. 279–340; and A. K. Burell, D. L. Officer, P. G. Plieger and D. C. W. Reid, *Chem. Rev.*, 2001, **101**, 2751. For examples of trimeric or lager porphyrin assemblies, see: P. Tecilla, R. P. Dixon, G. Slobodkin, D. S. Alavi, D. H. Waldeck and A. D. Hamilton, *J. Am. Chem. Soc.*, 1990, **112**, 9408; A. M. Brun, S. J. Atherton, A. Harriman, V. Heitz and J.-P. Sauvage, *J. Am. Chem. Soc.*, 1992,

114, 4632; F. Odobel and J.-P. Sauvage, *New J. Chem.*, 1994, **18**, 1139; S. Anderson, H. L. Anderson, A. Bashall, M. Mcpartlin and J. K. M. Sanders, *Angew. Chem., Int. Ed. Engl.*, 1995, **34**, 1096; A. V. Chernook, U. Rempel, C. von Borczyskowski, A. M. Shulgam and E. I. Zenkevich, *Chem. Phys. Lett.*, 1996, **254**, 229; C. A. Hunter and R. K. Hyde, *Angew. Chem., Int. Ed. Engl.*, 1996, **35**, 1936; C. M. Drain, K. C. Russell and J.-M. Lehn, *Chem. Commun.*, 1996, 337; Y. Kuroda, Y. Kato and H. Ogoshi, *Chem. Commun.*, 1997, 469; Y. Kuroda, N. Shiraishi, K. Sugou, K. Sasaki and H. Ogoshi, *Tetrahedron Lett.*, 1998, **39**, 2993; P. N. Taylor and H. L. Anderson, *J. Am. Chem Soc.*, 1999, **121**, 11 538; R. Takahashi and Y. Kobuke, *J. Am. Chem. Soc.*, 2003, **125**, 2372.

4 Y. Kuroda, K. Sugou and K. Sasaki, *J. Am. Chem. Soc.*, 2000, **122**, 7833; K. Sugou, K. Sasaki, K. Kitajima, T. Iwaki and Y. Kuroda, *J. Am. Chem. Soc.*, 2002, **124**, 1182.

5 Y. Kuroda, A. Kawashima, T. Urai and H. Ogoshi, *Tetrahedron Lett.*, 1995, **36**, 8449; Y. Kuroda, A. Kawashima and H. Ogoshi, *Chem. Lett.*, 1996, **57**; Y. Kuroda, A. Kawashima, Y. Hayashi and H. Ogoshi, *J. Am. Chem. Soc.*, 1997, **119**, 4929.

6 Y. Houminer, R. A. Fenner, H. V. Secor and J. I. Seemann, *J. Org. Chem.*, 1987, **52**, 3971.

7 The analyses and manipulation of the electronic and the fluorescence spectra in this work were performed by using the software SPANA developed in this laboratory, which is available from our web-site, http://www.poly.kit.ac.jp/~kinosekk/index.html.

8 The weak electronic interactions for these assemblies are observed in the Soret band region, where the observed spectra of the $\mathbf{P}^{n}\cdot(\mathbf{ZnP}_2)_4$ assemblies tend to broaden compared with those composed of the corresponding component spectra. For the spectroscopic effect of the multi-porphyrin interaction, see, for example: T. Nagata, A. Osuka and K. Maruyama, *J. Am. Chem. Soc.*, 1990, **112**, 3054; A. Osuka, N. Tanabe, S. Nakajima and K. Maruyama, *J. Chem. Soc., Perkin Trans. 2*, 1996, 199.

9 For the theoretical treatment of the multiple equilibrium processes, see: C. Tanford, *Physical Chemistry of Macromolecules*, John Wiley & Sons, New York, 1961.

10 Since the larger value of the binding constant gives practically the same theoretical curve fitting, the value determined by the present titration is regarded as a minimum estimate.

11 J. A. Blackburn, *Anal. Chem.*, 1965, **37**, 1000.

12 T. Förster, *Fluorenzenz Organische Verbindungen*, Vandenhoech and Ruprech, Göttingen, 1951; T. Förster, *Ann. Physik*, 1948, **2**, 55; T. Förster, *Discuss. Faraday Soc.*, 1959, **27**, 7. For an example of practical application for the energy transfer between porphyrins, see: J. L. Sessler, B. Wang and A. Harriman, *J. Am. Chem. Soc.*, 1995, **117**, 704.

13 The orientation factor should not be necessarily fixed as 2/3 owing to the motional constraints for the donor and acceptor in the present assemblies which is suggested by the existence of $^{A}\mathbf{ZnP}_2^{\#}$. This value was tentatively used for following reasons: (a) the antenna moiety which has an extremely unfavourable orientation such as $^{A}\mathbf{ZnP}_2^{\#}$ is expected to be minor; (b) a variation of the orientation factor of medium values results in minor error in the estimation of the distance because of the sixth root relationship, see, for example: B. Valeur, *Molecular Fluorescence*, Wiley-VCH Verlag GmbH, Weinheim, 2002.

14 P. J. Flory, *Statistical Mechanics of Chain Molecules*, John Wiley & Sons, Inc., New York, 1969.

15 During the examination of this article, one of the referees suggests that the Dexter mechanism may already have some weight in the energy transfer at a distance of 12–14 Å. If the $\mathbf{P}^{1}$ point in Fig. 9 is neglected due to the observed orbital perturbation, the upward deviation observed for the $\mathbf{P}^{5}$ assembly may be explained by the contribution of the Dexter mechanism as shown by the dashed line in Fig. 9. This attractive possibility is important for the further detailed investigation of assemblies which have the donor–acceptor distance in the transitional region for the Dexter and Förster mechanisms. See, for related discussions: P. Brodard, S. Matzinger, E. Vauthey, O. Mongin, C. Papamicael and A. Gossauer, *J. Phys. Chem. A*, 1999, **103**, 5858; S. Faure, C. Stern, R. Guilard and P. D. Harvey, *J. Am. Chem. Soc.*, 2004, **126**, 1253.

16 M.-S. Choi, T. Aida, T. Yamazaki and I. Yamazaki, *Chem. Eur. J*, 2002, **8**, 2667.